The Modeling of Diffuse Boundaries in the 2-D Digital Waveguide Mesh

Simon Shelley and Damian T. Murphy

***Abstract*—The digital waveguide mesh can be used to simulate the propagation of sound waves in an acoustic system. The accurate simulation of the acoustic characteristics of boundaries within such a system is an important part of the model. One significant property of an acoustic boundary is its diffusivity. Previous approaches to simulating diffuse boundaries in a digital waveguide mesh are effective but exhibit limitations and have not been analyzed in detail. An improved technique is presented here that simulates diffusion at boundaries and offers a high degree of control and consistency. This technique works by rotating wavefronts as they pass through a special diffusing layer adjacent to the boundary. The waves are rotated randomly according to a chosen probability function and the model is lossless. This diffusion model is analyzed in detail, and its diffusivity is quantified in the form of frequency dependent diffusion coefficients. The approach used to measuring boundary diffusion is described here in detail for the 2-D digital waveguide mesh and can readily be extended for the 3-D case.**

***Index Terms*—Acoustic materials, acoustic waveguides, acoustics, architectural acoustics, diffusion processes.**

I. Introduction

THE DIGITAL waveguide mesh (DWM) is an approach used to accurately model the propagation of sound waves in 2-D and 3-D acoustic systems. One advantage it has over geometrical room acoustic modeling techniques such as ray-tracing [1] and the image-source method [2] is that the complex phenomena of sound diffraction and wave interference are modeled inherently [3], [4]. The ability to model *diffuse* reflections at a boundary is important in any room acoustics modeling solution, as it has a significant effect on the resultant sound propagation.

Specular reflection of sound occurs at smooth boundaries with the result that the angle of the reflected sound wave is equal to the angle of incidence. Irregularly shaped acoustic boundaries result in diffuse reflections, causing a redistribution of the sound energy across a range of angles upon reflection. In the most extreme case, the energy is spread evenly in every direction, whatever the angle of incidence, and this is known as complete diffusion [5]. Diffuse reflection will result in the concentrated energy found at certain modal frequencies being attenuated as standing waves become less prominent due to the scattering of energy, at boundaries, away from the modal cyclic paths present in the room [6]. The scale of the irregularities of a boundary determines the range of frequencies for which the effect of diffusion occurs. In the case where these irregularities are very small compared to the wavelength of the incident sound wave, very little diffusion is observed, and the reflection tends to the specular case [7].

One method to implement diffuse reflections in a computer model for room acoustics simulations is to intricately build each individual boundary irregularity directly into the model. Large boundary irregularities can be modeled in this way with relative ease. However, this method becomes problematic when the roughness of the actual real boundary is relatively small scale and complex, making it difficult to measure and reproduce. If this is applied to a model of a room in order to predict its room impulse response, for example, a map of the roughness of every single diffuse boundary would be required, and this would be costly in effort and impractical to implement. A model is therefore required where the diffuse behavior of boundaries is approximated in a more general way using a statistical approach. Such a model should ideally be adjustable so that the diffusive effects of the simulated boundaries can be optimized to match those of a wide range of real, irregularly shaped boundaries as closely as possible.

The general diffusive properties of real boundaries can be measured and characterized by data, for example using scattering [8] and diffusion coefficients [9]. In turn, this data can be used when designing boundary diffusion models, allowing the characteristics of a particular material or boundary to be applied directly in the simulations. Scattering coefficients are suitable for geometric modeling techniques as they are compatible with the boundary scattering algorithms they currently use. Scattering coefficient data, however, only contains information about the quantity of energy that is moved from the specular direction and is not concerned with the more detailed diffusive characteristics of the boundary. Diffusion coefficient data, described in Section II, holds more information about the nature of scattering at a boundary. It is designed as a detailed measure of the diffusive quality of acoustic boundaries and diffusors; however, it is not compatible with the diffuse reflection algorithms currently used in geometric modeling techniques [10].

Methods exist for modeling diffuse reflections in ray-tracing and image-source models and are based on statistical approaches [11]. A commonly used technique is to change the direction of reflected waves (or rays) after they strike the boundary using a random probability distribution designed to distribute the reflected energy according to Lambert's Cosine Law [12]. This law states that the amount of reflected energy found at a particular direction from the point of reflection at the boundary is proportional to the cosine of the angle between the direction of the reflected energy and the normal of the boundary, irrespective of the incident angle of the sound wave.

Manuscript received November 22, 2006; revised October 4, 2007. This work was supported by the U.K. Engineering and Physical Sciences Research Council (EPSRC). The associate editor coordinating the review of this manuscript and approving it for publication was Dr. Rudolf Rabenstein.

The authors are with the Audio Lab, Intelligent Systems Group, Department of Electronics, York University, Heslington, York, YO10 5DD, U.K. (e-mail: sbs107@ohm.york.ac.uk; dtm3@ohm.york.ac.uk).

Digital Object Identifier 10.1109/TASL.2007.913407

Partial diffuse boundaries are modeled by allowing a proportion of the reflected rays to reflect in the specular direction. A random number is typically chosen between 0 and 1 in order to decide whether the boundary acts as diffuse or specular for each particular ray. If the number is above a certain threshold the reflection is diffuse, with the result that not all of the reflected energy is diffuse and a certain amount of the reflected energy is specular.

Previous work in implementing diffusing boundaries for a DWM details the successful implementation of a highly diffusive boundary in a 2-D mesh using a quadratic residue diffusor [13]. Another technique has been developed that simulates diffusion by randomly rotating incident waves as they approach the boundary of the mesh [14]. Although effective, neither method offers a complete, controllable, and accurate boundary diffusion model, and a full analysis of these techniques in previous work is limited.

The technique described in [14] allows for control over the diffusivity of the modeled boundary; however, the method is limited by an inherent error. The error, described in Section IV-A, is caused by differences between ideal and actual mesh configuration conditions, and results in undesirable inconsistency in diffusion results. An improvement to this boundary diffusion method, the *diffusing layer*, has since been introduced, eliminating the previously identified error [15]. In order that such models can be examined in more detail, a method to measure their diffusivity has also been described [16]. The diffusing layer approach is analyzed in detail using this measurement technique, and the data provided, based on diffusion coefficients, can be used as a reference when designing and simulating diffuse boundaries in a DWM.

This paper aims to clearly describe and present a detailed analysis of the diffusing layer model previously presented in [15]. These new results give a greater understanding of the behavior of the model and show that the model can be used to simulate diffuse boundaries, with properties comparable to that observed in real diffuse boundaries. In addition, a multilayered adaptation of the diffusing layer model is proposed which offers some control over the frequency dependency of the resultant diffusive characteristics. The methods described here can be used to measure and compare the diffusivity of any boundary implemented in a DWM. By following the guidelines in this paper, it is possible to test different diffuse boundaries designed for a 2-D DWM (and by extension a 3-D DWM) and to compare them with both each other and with real diffuse boundaries.

This paper is organized as follows. In Section II of this paper, the diffusion coefficient and its measurement and testing conditions are described. Section III revisits the DWM and the theory behind it, the diffusion layer method used in this paper is described in Sections IV and V, and finally a detailed study of this method is outlined in Section VI, and the results from this are presented and discussed.

II. Diffusion Measurement and the Diffusion Coefficient

In order to accurately measure the effects of the diffusion model presented in this paper, a procedure is proposed and implemented for measuring the diffusion coefficient at a DWM boundary. This is a simulated version of the method outlined by the Audio Engineering Society (AES) information document for room acoustics and sound reinforcement systems entitled "Characterization and measurement of surface scattering uniformity" (AES-4id-2001) [9]. The test for the diffusivity of a single-plane diffusor (one where the boundary displays distinct anisotropic behavior) is particularly well suited to the 2-D DWM case, as the diffusion is measured in one plane.

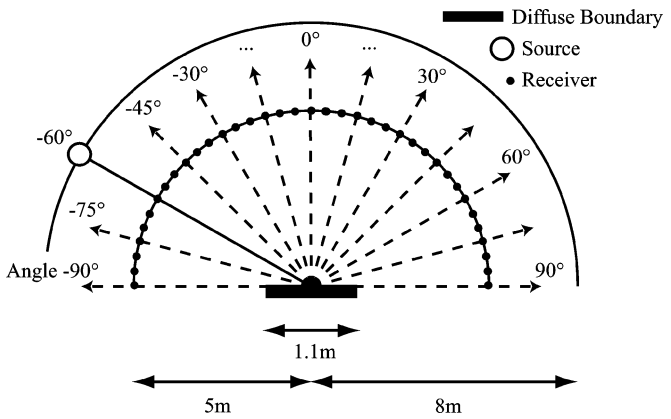

Fig. 1. Diagram showing the setup used for diffusion testing leading to the measurement of the diffusion coefficient. An impulse is applied at the source, which is rotated around the semicircle in order to obtain directional diffusion coefficients.

The *diffusion coefficient* is a measurement of the degree to which a boundary uniformly scatters incident sound. The *directional* diffusion coefficient d_θ can be measured for a particular angle of incidence. If a sufficient number of directional diffusion coefficients are obtained for different incident angles, they can be averaged to give the *random incidence* diffusion coefficient d of the boundary. The coefficient is measured for each third-octave band, giving information about the frequency dependency of the diffusion model. Diffusion coefficients are restricted to a minimum of 0, for totally specular reflections, and a maximum of 1, which signifies complete diffusion.

A. Measurement and Geometry

Ideally the real-world test should take place in a space with no acoustic boundaries, or an anechoic chamber, so that the results are not compromised by waves reflected from the perimeter boundaries of the room. It is possible to avoid this problem in a simulation by making the DWM sufficiently large relative to the distances between objects. Anechoic boundary implementations at the perimeter boundaries of the room may also be used, such as the *perfectly matched layer* [17].

In the test, a patch of the diffusive boundary is placed in the middle of the space, and receivers (microphones) are placed in a semicircle around its face, as illustrated in Fig. 1. An impulse is applied at a source, placed at an arbitrary point on another semicircle, with a radius greater than that of the receiver semicircle. In the case of a 2-D DWM, measurements can only be taken on a single plane. However, the test could be extended to a 3-D DWM, either taking measurements on two orthogonal planes or at different points on a hemisphere. Fig. 1 is a diagram showing the test geometry used to achieve the results presented in this paper, with the source in this case placed at an angle of -60 degrees to the normal of the sample boundary under test.

Distances between the boundary under test and source and receivers within the model should not be less than the distances

presented here. In the ideal case, distances are sufficiently large that true *far-field* conditions are achieved, such that the curve of wavefront emanating from the point source is allowed to travel far enough that it can be considered straight when it interacts with the sample boundary under test. If true far-field conditions cannot be achieved, it is necessary that at least 80% of the receivers are positioned outside the specular zone [9]. The suggested requirement according to [9] is that the receivers are separated by an angle of 5° at most, so that the spread of sound caused by the diffuse boundary is measured to a sufficiently high resolution to give accurate and useful data.

In order to calculate the diffusion coefficient of a certain diffusive object, impulse responses should be obtained for the space both with the diffusor present, $h_1(t)$ and in an empty space (without the diffusor), $h_2(t)$. It is then possible, at each receiver position, to measure the *diffusor impulse response*, or the impulse response that results only from the signal that has reflected from the diffusive boundary $h_3(t)$:

$$h_3(t) = h_1(t) - h_2(t). \tag{1}$$

If the tests are performed in the real world using a loudspeaker and microphone, it is suggested that the impulse response of the source/microphone pair is also measured, so that it can be taken into account in later calculations using a process of deconvolution [9]. However, this is not necessary in the DWM, as signals can be directly applied and measured.

The diffusor impulse response is calculated at each receiver position, and the frequency analysis of these results yields information about the diffusive qualities of the boundary for a given angle of incidence.

B. Calculation of the Diffusion Coefficient

For a fixed source position, the directional diffusion coefficient can be measured in each 1/3-octave band using the corresponding 1/3-octave RMS amplitude levels of the entire diffusor impulse response signals $h_3(t)$ measured at each of the n receivers. A form of autocorrelation is used on these measurements to give the directional diffusion coefficient d_θ as described in [9]. In this equation, L_i represents the RMS level calculated from the diffusor impulse response signal measured at receiver i for the 1/3-octave band under consideration:

$$d_\theta = \frac{\left(\sum_{i=1}^{n} E_i\right)^2 - \sum_{i=1}^{n} E_i^2}{(n-1)\sum_{i=1}^{n} E_i^2}, \quad E_i = 10^{L_i/10}. \tag{2}$$

In order to calculate the random incidence diffusion coefficient, directional diffusion coefficients are measured for source positions covering the entire semicircle, with a maximum angular resolution of 10° (as apposed to the maximum angular resolution of 5° which applies to the receiver positions). This angular resolution, according to [9], is enough to give a representative sample of results for a random incidence coefficient. The mean of these directional diffusion coefficients is then used to give the random incidence diffusion coefficient d for the material under test.

C. Discussion

The nature of the measurement technique used in the calculation of the diffusion coefficient requires that a finite sample of the diffuse boundary is used and this is problematic for two reasons. The first is that scattering effects will occur as a result of sound reflecting from the edges of the sample, with the result that even a plane specular reflecting boundary will cause some scattering and therefore yield a diffusion coefficient that is greater than zero. It is therefore good practice, when considering diffusion coefficient results from a diffuse boundary, to have at hand diffusion coefficients from a flat plane boundary of the same dimensions and measured under exactly the same test conditions for comparison.

The second issue again is a result of the finite size of the test sample and is caused by edge diffraction. If reflection from a plane boundary of finite size is considered, then a cutoff frequency is observed above which the acoustic boundary causes strongly specular reflection, when the wavelength of the sound is small relative to size of the boundary. Below this cutoff frequency, however, when the wavelength becomes larger relative to the size of the boundary, edge diffraction effects begin to dominate and the reflected sound from the boundary becomes less specular in nature, with less energy being reflected [18]. Eventually, if the wavelength is very large compared to the boundary, then no reflection will occur as the panel will have no effect on the sound wave. The effect is similar to that of a high-pass filter. The diffusion coefficient measurement technique is therefore only valid above this cutoff frequency. A method to calculate the cutoff frequency is proposed in [19] using a Fresnel integrals approximation. A similar attenuation of reflection strength below this cutoff frequency is observed when a diffuse boundary is considered.

For a test sample with width $2a$, where r_1 is the distance between the source, and the sample center at angle of incidence θ, r_2 is the distance between the receiver (preferably placed in the specular zone of reflection) and the sample center and c is the speed of sound, the -3-dB cutoff frequency, $f_{-3\mathrm{dB}}$ of the reflected sound is given as follows:

$$f_{-3\mathrm{dB}} = \frac{c\left(\frac{2r_1r_2}{r_1+r_2}\right)}{8a^2\cos^2(\theta)}. \tag{3}$$

III. Digital Waveguide Mesh

A. Background

The digital waveguide mesh is derived from the 1-D digital waveguide used extensively for physical modeling synthesis. The reader is referred to [20] and [21] for a thorough description and discussion of this area and a full derivation of the equations that follow in this section. Higher dimension mesh structures are constructed using bidirectional delay lines and scattering junctions which act as spatial and temporal sampling points within the modeled space. The digital waveguide mesh is analogous to the transmission line matrix (TLM) method [22]. The relationship between the two methods is explored in [23]. The sound pressure in a waveguide is represented by p_i, the particle velocity by v_i, and the impedance of the waveguide by Z_i, where $p_i/v_i = Z_i$. The input to a waveguide is termed p_i^+ and the output p_i^-. The signal $p_{J,i}^+$ therefore represents the incoming signal to junction J along the waveguide from the opposite junction i. Similarly, the signal $p_{J,i}^-$ represents the outgoing signal from junction J along the waveguide to the opposite junction i.

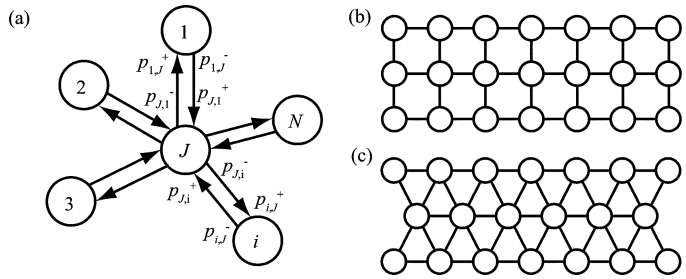

Fig. 2. (a) General scattering junction J with N connected waveguides for $i = 1, 2, \ldots, N$. (b) 2-D rectilinear mesh structure. (c) 2-D triangular structure.

By connecting scattering junctions together, it is possible to model wave propagation in 2-D and 3-D spaces, and different mesh topologies can be used to model the same physical structure. For instance, a 2-D space can be modeled using either a rectilinear mesh or a triangular mesh, diagrams of which can be seen in Fig. 2(b) and (c), respectively. The choice of topology dictates the number of neighbors that each scattering junction has.

The 1-D waveguide is a discretized formulation of the d'Alembert traveling wave solution to the 1-D wave equation

$$\frac{\partial^2 p(x,t)}{\partial t^2} = c^2 \frac{\partial^2 p(x,t)}{\partial x^2}. \tag{4}$$

This can be implemented using two bidirectional delay lines as indicated by one of the waveguide connecting elements of Fig. 2(a) between, for instance, junction J and junction i. The sound pressure of a propagating wave signal can be defined as the sum of these traveling waves or alternatively the input and output of this waveguide element

$$p_{J,i} = p^{+}_{J,i} + p^{-}_{J,i}. \tag{5}$$

As the waveguides are equivalent to bidirectional unit-delay lines, the input to scattering junction J at time index $n, p^{+}_{J,i}(n)$ is equal to the output from neighboring junction i into the connecting waveguide at the previous time step $p^{-}_{i,J}(n-1)$. Expressing this relationship in the z-domain gives

$$p^{+}_{J,i} = z^{-1} p^{-}_{i,J}. \tag{6}$$

For a lossless junction J, the sum of the input velocities is equal to the sum of the output velocities [24]

$$\sum_{i=1}^{N} \frac{p^{+}_{J,i}}{Z_i} = \sum_{i=1}^{N} \frac{p^{-}_{J,i}}{Z_i}. \tag{7}$$

From (5) and (7), and determining also that for a lossless junction J the sound pressures in all crossing waveguides are equal [24], the sound pressure p_J at J for N connected waveguides can be calculated using (8). A full derivation of this equation can be found in [25]:

$$p_J = \frac{2\sum_{i=1}^{N} \frac{p^{+}_{J,i}}{Z_i}}{\sum_{i=1}^{N} \frac{1}{Z_i}}. \tag{8}$$

Equation (5), (6), and (8) are collectively termed the scattering equations of the system. Models that use this implementation of the digital waveguide mesh are termed *W-models* or W-DWMs [26]. By applying an appropriate linear transformation, as described in [26] and in [27], an equivalent formulation can be derived in terms of junction pressure values only

$$p_J = \frac{2\sum_{i=1}^{N} \frac{p_i}{Z_i} \cdot z^{-1}}{\sum_{i=1}^{N} \frac{1}{Z_i}} - p_J \cdot z^{-2}. \tag{9}$$

The expression is also directly derived from a finite-difference time-domain (FDTD) formulation of the 2-D implementation of the wave equation. Digital waveguide meshes built using this alternative implementation, based on *Kirchoff* variables, are termed *K-models* or *K-DWMs* [26]. The advantage of the K-DWM approach is its greater computational efficiency over the W-DWM approach; however, it may be desirable to use the W-DWM approach to allow the use of scattering-based boundary termination options. The use of mixed models where both the K-DWM and the W-DWM implementations can be interfaced using a *KW-pipe* is discussed in [27]. This results in the formulation of a 2-D hybrid DWM [26], [27]. The work present in this paper is based on a W-DWM implementation as it is a requirement for the model to be able to access the incoming wave variables $p^{+}_{J,i}$ at certain junctions and for each time step. However, using the KW-pipe approach it is possible to formulate a hybrid mesh where those junctions whose incoming wave variables are required are implemented as W-DWM junctions and other junctions within the mesh are implemented as K-DWM junctions, therefore improving the overall efficiency of the model.

B. Mesh Limitations

There are a number of factors that currently limit DWM models as an optimal solution for full virtual acoustic applications. The first is dispersion error, where the velocity of the propagating wave is dependent upon both its frequency and direction of travel, leading to wave propagation errors and a mistuning of the expected resonant modes. The degree of dispersion error is highly dependent upon mesh topology and has been investigated in [28] and [29]. Both interpolated and triangular DWM topologies demonstrate dispersion characteristics that are substantially reduced to a function of frequency only, with frequency-warping techniques [30], [31] giving further significant improvements. For this reason, the triangular DWM is used for the implementation of the diffusion model discussed in this paper, although the method can readily be extended for any 2-D W-DWM implementation consisting of N-port scattering junctions. Over-sampling the mesh also offers improvements in this regard, such that the required bandwidth lies within accepted limits, typically $0.25 \times f_{\text{update}}$ for the rectilinear mesh, and that can be used as a benchmark figure for other mesh topologies [29], [32], where f_{update} is given by

$$f_{\text{update}} = \frac{c\sqrt{D}}{x}. \tag{10}$$

In this equation, c is the speed of sound, D is the dimension of the mesh, and x is the spatial distance between mesh junctions. Ultimately, f_{update} will dictate the quality of impulse response output from the mesh with large sample rates requiring denser meshes, more computer memory, and hence taking longer to run.

IV. Diffusion Model Using Circulant Matrices

Incoming signals to a scattering junction $p^+_{J,i}$ in a W-DWM are processed at each time step according to the scattering equations described in Section III-A, resulting in new outgoing signals that are received by the neighboring junctions at the next time step. These signals can be considered as vectors representing a traveling wavefront. These vectors have directions $\hat{p}_i$ that are equal to the directions of the connected waveguides. Provided that the vectors evenly span a circle, their directions can be calculated as follows:

$$\hat{p}_i = \begin{bmatrix} \cos\left((i-1)\frac{2\pi}{M}\right) \\ \sin\left((i-1)\frac{2\pi}{M}\right) \end{bmatrix} \tag{11}$$

where $i = 1, 2, \ldots, M$, equal to the number of connecting waveguides at the scattering junction.

The magnitudes of the vectors are given by the incoming signal values $p^+_{J,i}$. Therefore, the direction ϕ of the wavefront at the junction p_J is

$$\phi = \angle\left(\sum_{i=1}^{N} p^+_{J,i} \cdot \hat{p}_i\right). \tag{12}$$

It is possible to redistribute these signals so that the direction of travel ϕ of the wave at that particular junction is altered by an arbitrary angle φ. Care must be taken however to ensure that signal power and strength is conserved and that the model remains stable. The altered direction of the wave ϕ' is therefore

$$\phi' = \phi + \varphi. \tag{13}$$

One approach for modeling boundary diffusion in the DWM, introduced in [14] is to multiply the incoming signals or vector magnitudes at a boundary by circulant matrices in such a way that the resultant directions of the traveling waves ϕ' are randomly altered at each boundary junction just before they are reflected.

A circulant matrix is a square matrix where each row vector is cyclically shifted by one element to the right relative to the proceeding row vector. Circulant matrices have been previously used in the field of audio signal processing, although in a different way, providing a special class of *feedback delay networks* (FDNs) [33]–[35]. FDNs are used in the design of digital reverberation effects based on delay lines interconnected in a feedback loop. The feedback signals are processed using a matrix known as the *feedback matrix*. It is important that such systems show stability, and this is controlled by the design of the feedback matrix. It is also useful to be able to provide lossless prototypes as a starting point in the FDN design [35]. One approach that can be used in the design of the FDN is to use a circulant matrix, which can be made both stable and lossless by positioning the associated eigenvalues on the unit circle [36]. The positions of the eigenvalues can then be used to control the distribution of the resonant peaks and other properties of the resulting artificial reverb tail [37]. It should be noted that the goal of FDNs however, is to provide reverberation for a sound as a perceptual effect, rather than accurately modeling a particular acoustic space which is the ultimate goal of the DWM described in this paper.

In this application, the circulant matrix in the DWM is used to rotate the direction ϕ of the traveling waves at each boundary junction, by a different angle at each time step. The design and implementation of the circulant matrices is detailed in Section V. If this angle φ is varied using an appropriate random function, the energy of the propagating sound waves is effectively diffused as it travels through the boundary junctions. The greater the range of angles by which the propagating wavefronts are rotated, the greater the spread of energy upon reflection. Note that for any angle of incidence, this spread of energy will focus around the specular angle of reflection provided that the mean of the applied random function is 0°.

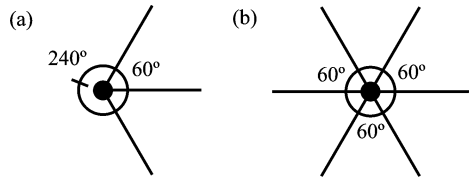

Fig. 3. (a) Three-port boundary junction and (b) a six-port junction with connecting waveguides.

A. Rotation Error

Connecting waveguides at the boundary junctions of a 2-D DWM are generally not distributed uniformly around the junction, meaning that they are not all separated by equal angles. An example of this is illustrated in the diagram of a three-port boundary junction from a 2-D triangular mesh shown in Fig. 3(a). Similarly, the case also exists where a boundary junction is connected to only one neighbor, and hence there is no possibility for any rotation of an incoming signal.

The nature of the circulant matrix transformation technique means that it is only consistent and without error if the connecting waveguides are uniformly distributed around the junction within the DWM, an example of which is shown in Fig. 3(b). Hence, due to a nonuniform distribution of connecting waveguides at a boundary junction, inconsistencies will occur when the incoming signals are manipulated by the circulant matrices. This is referred to as *rotation error*, and analysis shows [14] that there is a complex nonlinear mapping between the intended (ideal) angle of rotation and the actual (real) angle of rotation that is dependent on two factors. The first is the amount of rotation that is applied in the ideal case, and the second is the angle of approach of the incoming waves. The effects of this discrepancy become less extreme as the number of waveguides connected to a boundary junction increases. This implies that there are nonuniform distribution inconsistencies in this proposed DWM diffusion model, as different types of boundary junctions exhibit different diffusive characteristics. The error becomes particularly apparent when modeling boundaries with low diffusivity, as small angles of rotation will tend to be distorted into large angles.

V. Diffusing Layer

Rotation error occurs when the circulant matrix transformation technique is applied to boundary junctions in the DWM. However, if the same method is applied to a standard N-port air-junction, then the error is eliminated because the connecting waveguides are uniformly distributed, being separated by equal angles. In the case of a 2-D triangular DWM, such junctions have six connecting waveguides, separated by angles of 60°, as

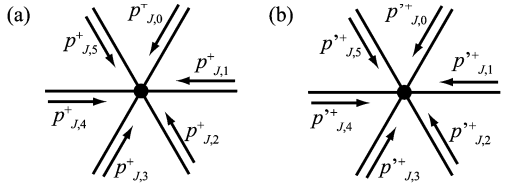

Fig. 4. Incoming signals at a diffusing junction J (a) before rotation and (b) after rotation. The resulting incoming signals $p'^{+}_{J,i}$ are then used in the scattering equations rather than the original signals $p^{+}_{J,i}$.

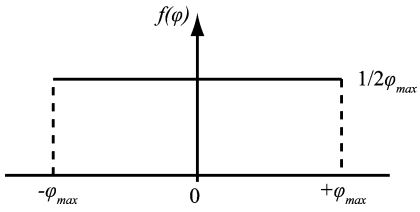

Fig. 5. Probability density function of the uniform distribution used in the diffuse boundary model.

shown in 3(b). This is the ideal case for the circulant matrix rotation technique, as the connecting junctions are evenly distributed around the junction and hence there is no rotation error. Therefore, by applying these rotations at air-junctions *adjacent* to the boundary, rather than the boundary junctions themselves, it is possible to achieve diffusion without inherent rotation error.

As a result of this *diffusing layer* technique, waves that approach the boundary are usually rotated twice. Once as they approach the boundary and a second time as they travel away from it after being reflected. This can be compensated for by halving the required rotation angles at the junctions adjacent to the boundary. Undesirable effects may occur, however, when large rotation angles are applied because waves may be rotated more than twice or even just once, depending on the angle of approach and the amount of rotation that is applied.

A. Implementation in the 2-D Triangular DWM

The direction of wave travel, ϕ at a six-port air-junction in a 2-D DWM can be rotated by an angle φ if the incoming signals are multiplied with a circulant matrix $\mathbf{A}$, whose coefficients can be calculated using the set of eigenvalues X, described by (14). To achieve rotation, the eigenvalues are arranged symmetrically and are distributed along the unit circle (14), resulting in signal conservation and stability, as described in [14]. A detailed study of circulant matrices and their associated eigenvalues is given in [38]:

$$X = [1 \quad e^{j\varphi} \quad e^{j2\varphi} \quad -1 \quad e^{-j2\varphi} \quad e^{-j\varphi}]. \tag{14}$$

An inverse discrete Fourier transform, performed on these eigenvalues, yields six real numbers that sequentially make up the first row of coefficients $x_0, \ldots, x_5$ in the circulant matrix $\mathbf{A}$. The coefficients in subsequent rows can be calculated as follows:

$$\mathbf{A} = \begin{bmatrix} x_0 & x_1 & \ldots & x_5 \\ x_5 & x_0 & \ldots & x_4 \\ \ldots & \ldots & \ldots & \ldots \\ x_1 & \ldots & x_5 & x_0 \end{bmatrix} \tag{15}$$

The resultant direction of the wavefront at each air-junction, ϕ (defined in (12)) can now be rotated by the angle φ by multiplying the matrix A with the incoming signals $p^{+}_{J,i}$ to produce a new set of incoming signals, $p'^{+}_{J,i}$ (16). This process is illustrated in Fig. 4.

$$\mathbf{A} \begin{bmatrix} p^{+}_{J,0} \\ p^{+}_{J,1} \\ \vdots \\ p^{+}_{J,5} \end{bmatrix} = \begin{bmatrix} p'^{+}_{J,0} \\ p'^{+}_{J,1} \\ \vdots \\ p'^{+}_{J,5} \end{bmatrix}. \tag{16}$$

The new incoming signals at the diffusing junctions $p'^{+}_{J,i}$ are subsequently used in the scattering equations [(5), (6), and (8)], and the simulation continues until the next time step when the next set of incoming signals at each junction are determined and the rotation process described here repeats itself.

Diffusion is simulated by randomly altering the amount of rotation φ of the incoming signals at each of the chosen diffusing junctions at each sample time step, before the scattering equations are calculated. The rotation is applied to the junctions found adjacent to the boundary junctions. A different angle of rotation is randomly chosen for each junction and at each time step, according to a *probability distribution*. The amount of diffusion that is modeled can be controlled by limiting the algorithm to a range of angles. For instance, to simulate a relatively smooth wall the maximum random angle that can be selected is set to $\pm 5^{\circ}$. Greater diffusivity can be achieved by increasing this angle. In the diffusion model implementation used in this paper, the rotation angle φ is selected at random according to a uniform probability distribution function $f(\varphi)$ given by (17) and illustrated by Fig. 5, with the result that the rotation angle is limited to $\pm\varphi_{\max}$ degrees and the mean of the distribution is zero:

$$f(\varphi) = \begin{cases} \frac{1}{2\varphi_{\max}}, & \text{for } -\varphi_{\max} \le \varphi \le +\varphi_{\max} \\ 0, & \text{for } \varphi < -\varphi_{\max} \text{or} \varphi > +\varphi_{\max} \end{cases} \tag{17}$$

VI. Study of the Diffusing Layer Technique

A series of tests are performed designed to give a detailed analysis of the diffusing layer approach to modeling diffusion at the boundary of a 2-D triangular DWM. The tests are described in this section and the results are presented and discussed.

A. Modal Analysis in a 2-D Lossless DWM

The method proposed in Section V of this paper, in which rotations are performed at junctions adjacent to the boundary, is referred to here as the *diffusing layer* method. The method originally proposed in [14] and described in Section IV, where rotations are performed at the actual boundary junctions of the mesh themselves, is referred to here as the *diffusing boundary* method. In this section, the two methods are compared by defining two identical 2-D DWM structures. In one structure, the *diffusing layer* method is implemented at each of the boundaries and this structure is named Model A. In the other structure the *diffusing boundary* method is implemented at each of the boundaries. This second structure is labeled Model B. During the simulations that follow, the angle of rotation is selected at random according to a uniform probability density function (17), limited to a specified range of angles by altering the maximum angle of

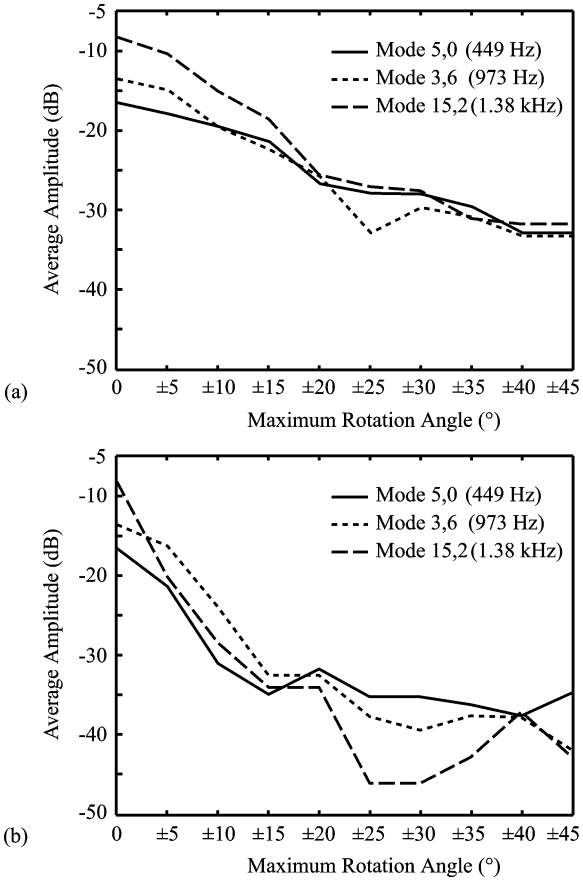

Fig. 6. Graphs showing the average amplitudes of the outputs from (a) Model A and (b) Model B at three modal frequencies for each 4-s simulation.

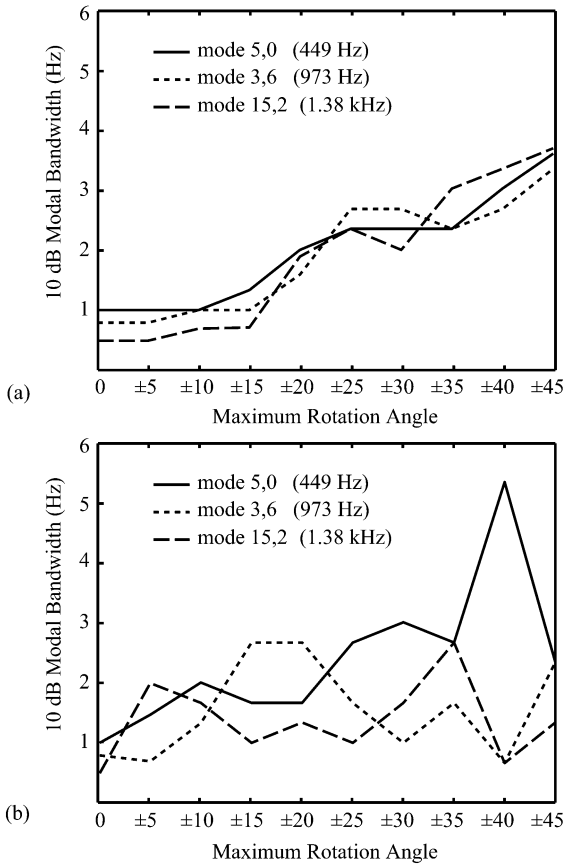

Fig. 7. Graphs showing the 10-dB modal bandwidths of the outputs from (a) Model A and (b) Model B at three modal frequencies for each 4-s simulation.

the probability function $\varphi_{\max}$. The mean of the function always remains constant at zero.

The two structures are rectangular in shape, and the 2-D triangular DWM is used. The length of each structure is 1.91 m and the width 1.10 m, and f_{update} is set at 44.1 kHz, giving an internodal distance x of 0.0110 m according to (10). Ten consecutive simulations, each lasting 4 s, are performed on each mesh, each with an increasing level of diffusivity implemented at every boundary. At the start of each simulation, the meshes are excited with a low-pass filtered impulse applied near a corner and the outputs are obtained at a junction at the opposite corner. The maximum angle used in the probability function is 0° in the first simulation, where effectively no diffusion model is applied. This maximum diffusion angle increases at each simulation by ±5° until the final test when it reaches a maximum of ±45°.

In order to compare the effects of the simulated boundary scattering in the two models, three modal frequencies (449 Hz, 973 Hz, and 1.38 kHz) are arbitrarily selected for analysis. Increased scattering at the boundaries results in the average amplitudes of the output being diminished at modal frequencies. As well as this, the bandwidth of energy found at the modal frequencies increases as energy is spread away from the modal frequencies [6]. The average amplitude at each of these three modal frequencies, for each simulation, in both Model A and Model B is shown in Fig. 6. 10-dB modal bandwidths for the same three modal frequencies are shown in Fig. 7.

B. Discussion

When the diffusion algorithm is limited by a maximum angle of just 5°, the average amplitude of the output at the selected modal frequencies is sharply attenuated in Model B in comparison to the case where no boundary diffusion is modeled at all, indicating a relatively high diffusivity at the boundaries. In Model A, however, this drop in amplitude observed at the modal frequencies is not so great. For instance, the average amplitude at the modal frequency of 1.38 kHz is attenuated by 12.0 dB in Model B; however, it is only attenuated by 2.1 dB in Model A. As the limit of the angles is increased, the observed diffusivity of Model B appears to fluctuate to varying degrees at different modal frequencies. Some fluctuation is also observed in Model A, but to a lesser extent, and the diffusivity at the boundaries increases with consistency.

This difference in consistency of the two models can be observed at other modal frequencies and is evidence that the rotation error has a significant effect on the diffusion model. The mesh structure is rectangular in shape and owing to the nature of its implementation and the triangular topology of the mesh, the boundary junctions found along the length of the structure differ to the boundary junctions located along its width in terms of their number of connecting waveguides. The inconsistencies observed between different modal frequencies in Model B are a result of the inconsistent nature of the rotation error when rotations are applied to boundary junctions with differing numbers of connecting waveguides, as discussed in Section IV-A.

These inconsistencies are also explained by the fact that rotation error is dependent in part by the angle of incidence of the waves. This is a factor because the angle of incidence of reflections of a standing wave within the structure vary depending on its cyclic path. The sharp increase in amplitude levels at modal frequencies in Model B for relatively small angles of rotation in comparison with Model A is again a result of the rotation error because small angles of rotation are distorted into large angles, as discussed in Section IV-A. The results show that using the diffusing layer method described in Section V, a more controlled and consistent diffusion model can be achieved. This is particularly true for small ranges of diffusion angles.

The improved diffusion exhibited by this new method can be explained by the elimination of the rotation error, implying that small rotation angles are no longer translated into larger angles. This has a clear advantage when modeling boundaries with low diffusivity, commonly found in real-world materials.

C. Early Reflection Testing

The early reflections are the stronger, more distinct, and widely spaced reflections that are found at the beginning of the impulse response. They are typically found in the first 100 ms, although this is dependent on the volume of the space and the geometrical arrangement of the source, receiver, and boundaries. The early reflections help the listener to determine source location and information about the geometry of the space itself. Diffusivity at the boundaries of the room will have some effect on the early reflections. Generally, small-scale boundary diffusion results in a slight diminution in the strength of the early reflections as well as some smearing as the energy distribution in the space is spread out more evenly. However, the overall geometry of the room is not changed; therefore, the early reflections should not be any different in the respect of timing and their dominance is preserved.

In order to test that the diffusing layer implementation behaves correctly and does not result in inaccurate early reflections being produced by the room model, a simple 2-D DWM structure is defined. The structure is again rectangular in shape, the dimensions of which are 8 m by 6 m. Again, f_{update} is set at 44.1 kHz, giving an internodal distance x of 0.0110 m. Three simulations are performed, each with a length of 3000 samples, or 0.068 s. Impulse responses are obtained for each simulation by exciting the mesh with a low-pass filtered impulse near one corner and outputs are generated from a junction near the opposite corner. In each simulation, the diffusing layer is applied at the boundaries of the structure, with the limited range of rotation angles set to 0° in the first simulation, 45° in the second simulation, and 90° in the third. These boundary models are referred to as MA00, MA45, and MA90, respectively.

Fig. 8 shows the early parts of the impulse responses obtained using the simulation. The signals have been low-pass filtered at a quarter of the sampling rate, as the DWM typically is limited to giving valid results in this bandwidth only as described in Section III-B. It can be seen that in each test the peaks caused by early reflections are largely preserved but become slightly attenuated as the range of rotation angles in the diffusion model is increased. For instance, the second peak, which is the first first-order reflection to reach the receiver, is attenuated as a result of the 45° diffusion implementation by just 4.95% and by 5.41% when the maximum angle is set to 90°. Likewise, the third peak (the second first-order reflection) is reduced by 5.30% when the maximum rotation angle is set to 45° and by 6.50% when it is set to 90°.

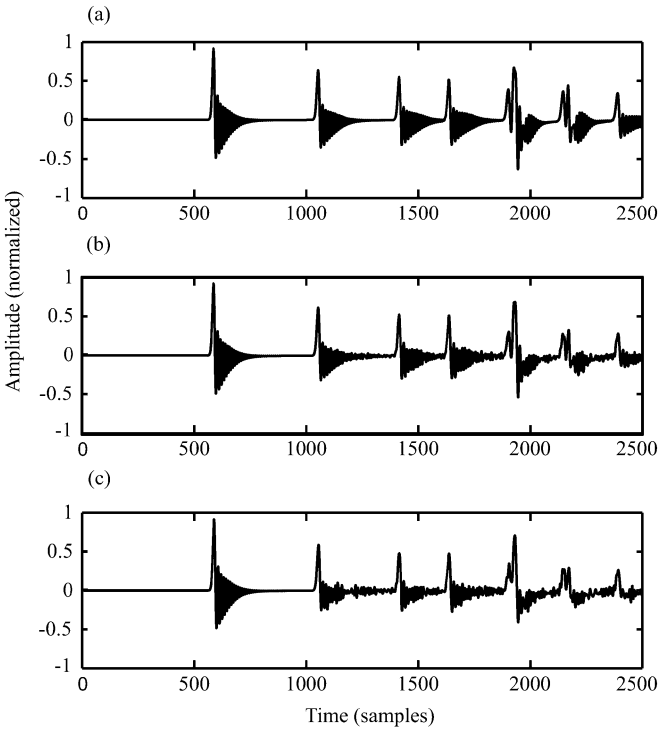

Fig. 8. Graphs showing early part of impulse responses for room simulations with boundary diffusion models (a) MA00, (b) MA45, and (c) MA90 implemented at each boundary.

D. Measurement of Diffusion Coefficients

In order to measure the diffusion coefficients for the diffusing layer model across a range of incident angles for varying levels of diffusivity, a test is prepared as described in Section II-A and illustrated in Fig. 1. A 2-D triangular DWM is used with $f_{\text{update}} = 44.1$ kHz. The diffusing layer model is implemented at one edge of a rectangular block placed in the center of the mesh. A series of simulations are performed for varying levels of diffusivity. A low-pass filtered impulse is applied as the source, which is located at a range of incident angles, from $-80°$ to 0°, with respect to the normal of the boundary sample under test. The impulse is applied at a distance of 8 m from the center of the diffuse boundary in each simulation. Receivers are placed in a semicircle so that each receiver is a distance of 5 m from the center of the diffuse boundary. An angular resolution of 5° is used, with the total number of receivers therefore being 37, running from $-90°$ through to 90° with respect to the normal of the boundary. Each simulation is run for sufficient time to allow the propagating signal to travel from the source to the boundary sample under test and then to subsequently reflect and propagate to the receivers. The DWM used is sufficiently large that waves reflecting from the perimeter boundaries do not interfere with the results. In order to obtain the diffusor impulse response at each receiver position and for each source position, an impulse response is measured in an empty mesh, so that the direct responses from source to receiver can be removed according to (1).

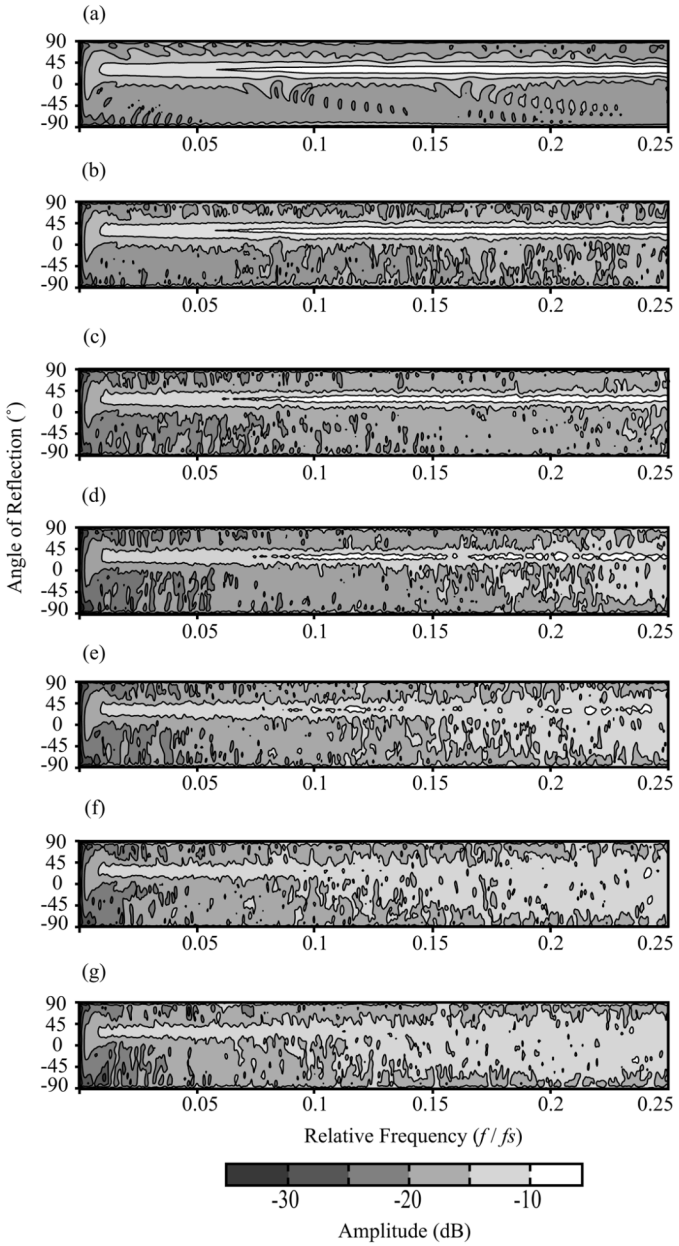

Fig. 9. Contour plots showing reflection magnitude for -30° incidence, varying with angle of reflection across the semicircular range of receivers with (a) MA00, (b) MA15, (c) MA30, (d) MA45, (e) MA60, (f) MA75, and (g) MA90.

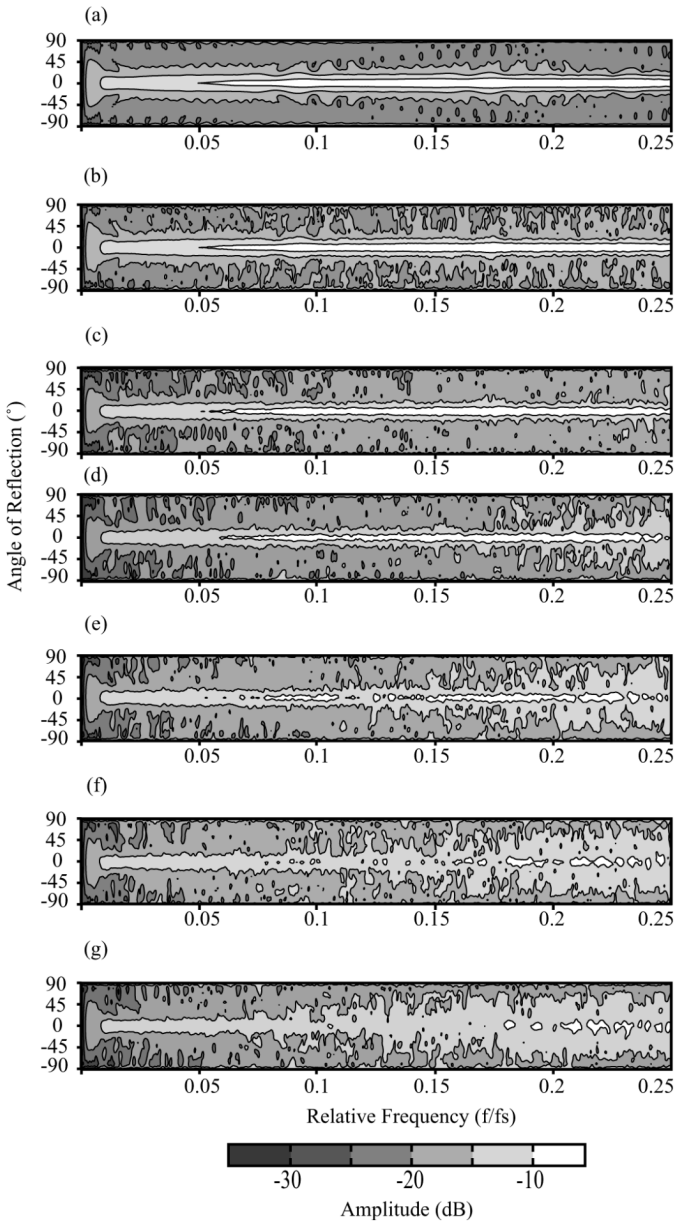

Fig. 10. Contour plots showing reflection magnitude for normal incidence varying with angle of reflection across the semicircular range of receivers with (a) MA00, (b) MA15, (c) MA30, (d) MA45, (e) MA60, (f) MA75, and (g) MA90.

The diffusing layer model is tested for seven different levels of diffusivity, analogous to seven acoustically reflective materials with different diffusive properties. The materials are modeled using a uniform probability function to select the random angles of rotation, with maximum rotation angles of $0^\circ, \pm 15^\circ, \pm 30^\circ, \pm 45^\circ, \pm 60^\circ, \pm 75^\circ$, and $\pm 90^\circ$. For later reference, these are labeled MA00, MA15, MA30, MA45, MA60, MA75, and MA90, respectively. Theoretically, the higher the maximum angle in the random function used to control the diffusion, the greater the diffusivity of the material.

E. Results and Discussion

Figs. 9 and 10 show a frequency analysis of the diffusor impulse responses for angles of incidence -30° and 0° (normal incidence), respectively, in the form of contour plots. For each of the 37 receiver angles, the diffusor impulse response is zero-padded and a 4096-point fast Fourier transform (FFT) is applied. The results are presented using an x-axis relative frequency scale up to a quarter of the sampling rate.

Patterns of constructive and destructive interference are evident in the frequency analysis of the diffusor impulse responses where a specular material (MA00) is used. However, when diffuse materials are used this behavior is eliminated and the spectrum becomes more noise-like.

It can be seen in these graphs that as the maximum angle is increased for the uniform random distribution function, the energy observed at the angle of specular reflection (30° in Fig. 9 and 0° in Fig. 10) reduces, and the total energy observed at other angles increases. For every test, the amplitude of the reflected energy

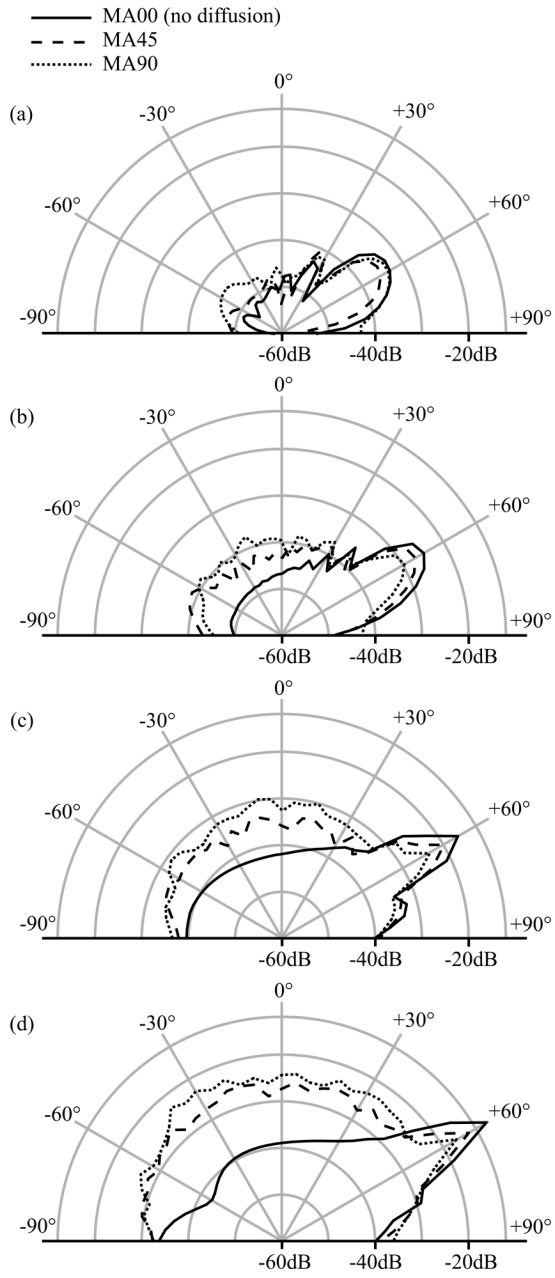

Fig. 11. Polar responses showing scattering of reflected sound energy for −60° incidence in (a) 1000 Hz, (b) 2000 Hz, (c) 4000 Hz, and (d) 8000 Hz 1/3 octave bands.

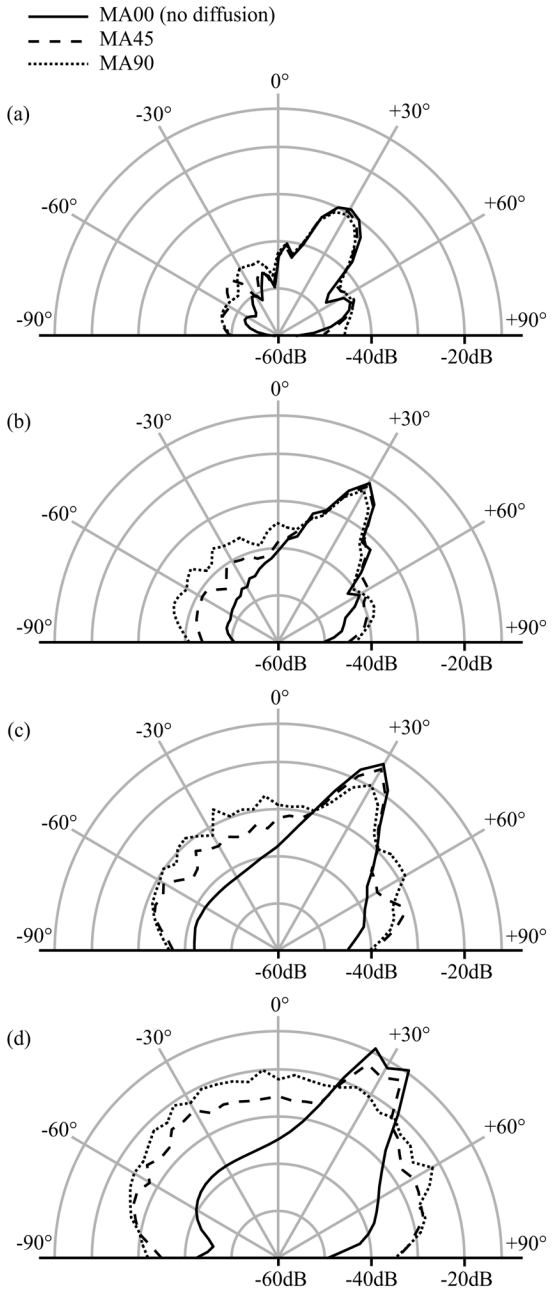

Fig. 12. Polar responses showing scattering of reflected sound energy for −30° incidence in (a) 1000 Hz, (b) 2000 Hz, (c) 4000 Hz, and (d) 8000 Hz 1/3 octave bands.

diminishes in the low-frequency region due to the wavelength of the incident sound wave being large in comparison to the width of the diffusing object, as discussed in Section II-C. According to (3), the width of the object, 1.1 m, implies that an incident sound wave will not be reflected effectively below 872 Hz (a relative frequency value of 0.0198). It is important to note that the energy in this low-frequency region is not lost as a result of the diffusion model however, but rather it is not reflected due to the finite size of the test sample.

The resulting data can also be represented using polar plots as shown in Figs. 11–13. This time, the data is given for angles of incidence -60°, -30° and 0°, respectively. These graphs show the RMS levels of the diffusor impulse responses computed at four different 1/3 octave bands with center frequencies at 1000, 2000, 4000, and 8000 Hz. These are chosen so that the behavior of the model can be observed over a range of frequencies. It can again be seen that the amount of energy that is reflected diminishes at lower frequencies, below 2 kHz.

This information is used to calculate the diffusion coefficients for the seven different boundary materials. The autocorrelation of the measurements taken at each receiver for a specific angle of incidence gives the corresponding directional diffusion coefficient as detailed in II-B. Fig. 14 shows directional diffusion coefficients for each boundary model for angles of incidence running from -80° to 0° with respect to the normal of the boundary under test. The diffusion coefficients in these graphs are calculated using the RMS levels at four different 1/3 octave bands

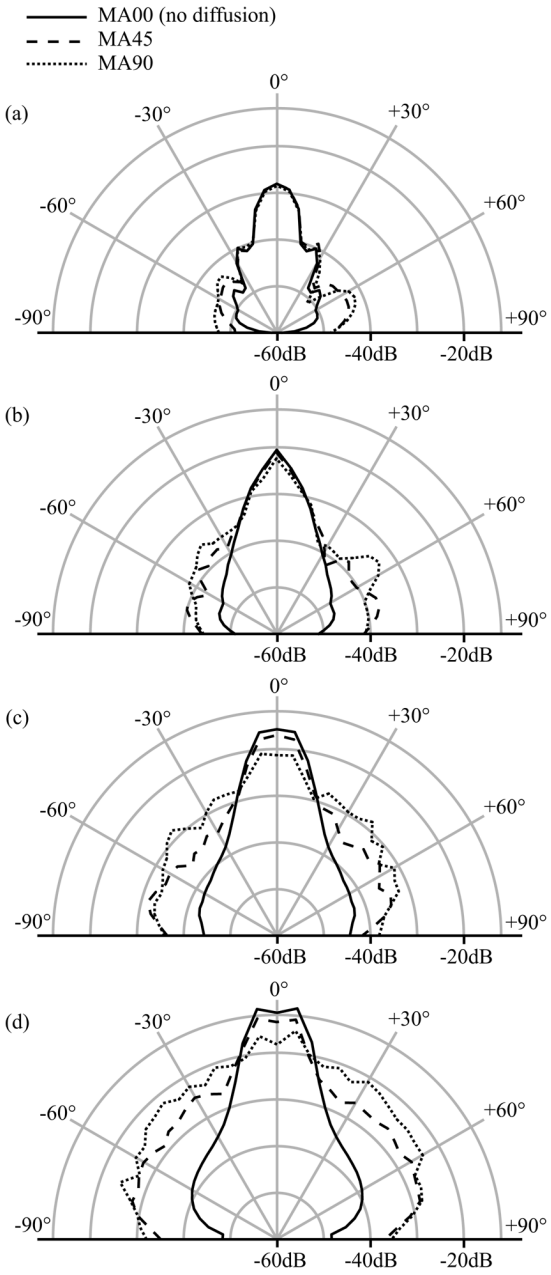

Fig. 13. Polar responses showing scattering of reflected sound energy for normal incidence in (a) 1000 Hz, (b) 2000 Hz, (c) 4000 Hz, and (d) 8000 Hz 1/3 octave bands.

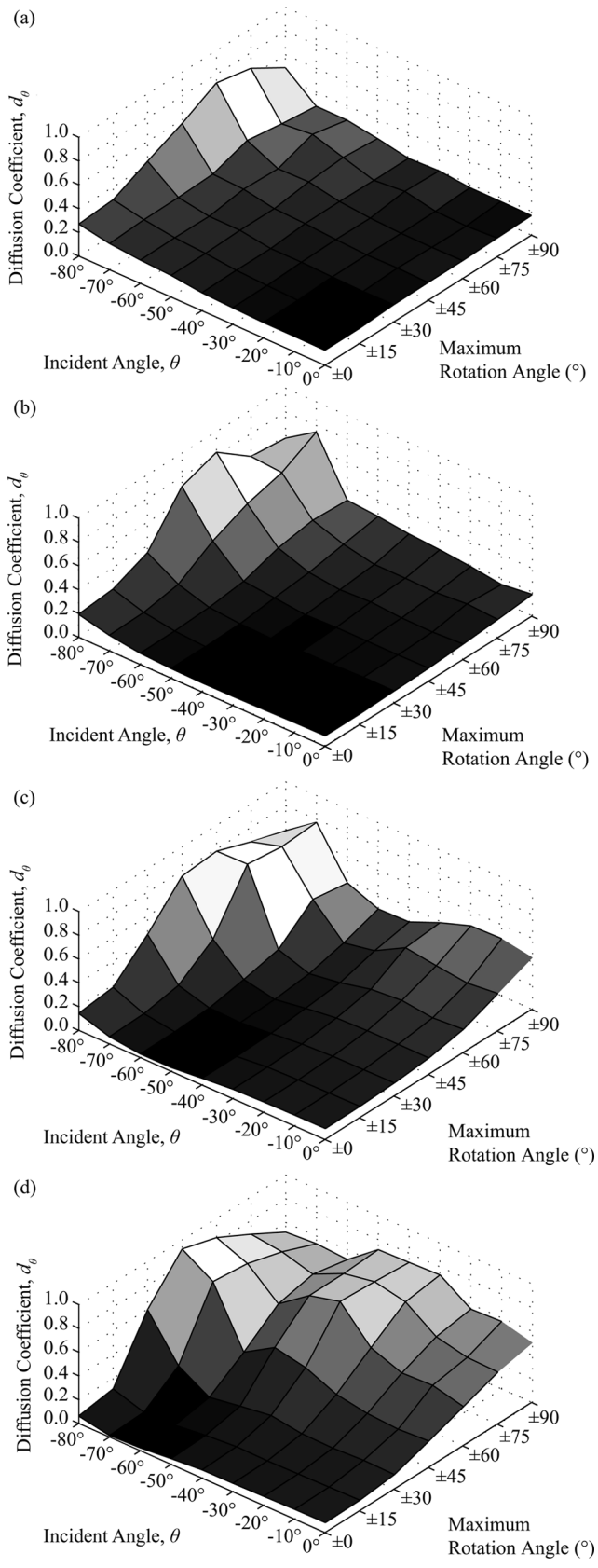

Fig. 14. Graphs showing directional diffusion coefficients for the modeled boundaries in (a) 1000 Hz, (b) 2000 Hz, (c) 4000 Hz, and (d) 8000 Hz 1/3 Octave bands.

with center frequencies equal to those chosen for the polar responses (Figs. 11–13). The graphs show a rise in diffusion coefficient for most angles of incidence as the maximum rotation angle used in the boundary models increases. This rise in diffusion coefficient is very slight, however for the lower 1/3 octave frequency bands. At 1000 Hz, the diffusion coefficients rise from 0.17 on average across the range of incident angles, to just 0.24 on average. At 8000 Hz however, the average of the diffusion coefficients rises from 0.06 (MA00) to 0.61 for the MA90 material. This again shows that the diffusion model is less effective at the lower frequencies. The rise in diffusion coefficients generally levels out at a maximum rotation angle of 60°. Further tests show that increasing the maximum rotation angle further

TABLE I
TABLE SHOWING RANDOM INCIDENCE DIFFUSION COEFFICIENTS FOR THE SEVEN BOUNDARY MODELS

	Modeled Boundary Diffusion Coefficients						
1/3 Octave Band(Hz)	$MA00$	$MA15$	$MA30$	$MA45$	$MA60$	$MA75$	$MA90$
1000	0.17	0.18	0.20	0.23	0.26	0.27	0.24
1250	0.15	0.15	0.18	0.22	0.26	0.29	0.24
1600	0.12	0.13	0.16	0.22	0.26	0.27	0.26
2000	0.11	0.12	0.15	0.22	0.27	0.28	0.26
2500	0.10	0.10	0.13	0.21	0.26	0.28	0.31
3150	0.09	0.09	0.13	0.21	0.27	0.32	0.33
4000	0.08	0.09	0.13	0.20	0.27	0.34	0.40
5000	0.08	0.08	0.13	0.21	0.31	0.39	0.45
6300	0.07	0.08	0.13	0.23	0.35	0.50	0.58
8000	0.06	0.07	0.14	0.30	0.43	0.54	0.61
10000	0.06	0.07	0.19	0.41	0.57	0.60	0.60

does not cause any significant rise in the measured diffusion coefficient. For incident angles with the greatest absolute value (-90° and -80°) measured diffusion coefficient is unexpectedly high, particularly for the boundary models MA45, MA60, and MA75 (peaking at 0.92 in the 8000 Hz 1/3 ocrave band). The cause of this inconsistency is not obvious. One reason may be that incident waves from these shallow angles are far more likely to be rotated more than twice as they pass over the length of the diffusing material. Inconsistencies at shallow angles may also be caused by reflections of sound waves from the edge of the strip of diffusing material and also by diffraction effects.

Once sufficient directional diffusion coefficients are collected, then the random incidence diffusion coefficient is determined by calculating their mean [9]. Table I shows the calculated random incidence diffusion coefficients for the seven modeled diffusing layer boundaries. The diffusion coefficients are given for the 1/3 octave bands with central frequencies running from 1 kHz to 10 kHz. These results are also displayed in the form of a 3-D graph shown in Fig. 15(a).

It is clear from the random incidence diffusion coefficient data that the diffusion model becomes more effective as the frequency of the incident sound wave increases. Generally, sound waves with a frequency of 5000 Hz and above are diffused most effectively. As can be expected, the diffusive effect of the diffusing layer model increases as the maximum rotation angle that can be selected by the uniform probability function is increased. The data also indicates that there is an upper threshold, beyond which the random incidence diffusion coefficients do not increase. A peak in the data of 0.61 is observed in the 8-kHz 1/3 octave band, when the maximum angle of the diffusion model is set to $\pm 90^\circ$. In the 10-kHz 1/3 octave band, where the diffusion model is more effective, a peak in the random incidence diffusion coefficient of 0.60 is reached when the maximum rotation angle of the diffusion model is set to $\pm 75^\circ$. As the maximum rotation angle is increased, the measured random incidence diffusion coefficient does not increase above this value.

The implementation of diffusing layer boundaries in a DWM can have a significant audible effect on its output and results in a more natural reverberant sound. A demonstration of this can be heard in presentation sound examples which are available online [39]. These were produced using 2-D DWMs to simulate sound reverberation in identical models with different levels of diffusivity at the boundaries, including one with specular boundaries for comparison. In these examples, a spreading of energy away from the modal frequencies is clearly audible as the modeled boundary diffusion is increased, particularly at the higher frequencies. The impulse response is therefore more noise-like in the higher frequencies, and the ringing modal frequencies cannot be heard so clearly.

F. Comparison With Real-World Boundary Diffusion

In the study of acoustics, it is observed that the size of the largest irregularities in a randomly rough reflective boundary must be at least of a similar size, or greater than half the wavelength of the incident sound waves in order for diffuse reflection to occur [7]. As an example, it would take irregularities of 39 cm or more in size to result in the effective diffusion of a sound wave at 440 Hz for a randomly rough wall. Such large irregularities can be included in the geometrical definition used in a room acoustic model with ease, as they are large compared to the boundaries of the room. The results presented in this paper demonstrate that the diffusing layer model, for a 2-D DWM of triangular topology and sampled at 44.1 kHz, displays a range of diffusive properties depending on the maximum angle that can be selected by the probability function of the modeling algorithm. The high-frequency nature of the model shows that it effectively models random rough boundaries with maximum irregularities of between 3 and 8 cm in size.

Fig. 15(b) and (c) shows frequency-dependent random incidence diffusion coefficient data for an adapted version of the diffusing layer model. The test conditions in these cases are identical to those applied to the original diffusing layer model; however, two and three layers, respectively, of diffusing junctions adjacent to the boundary are implemented rather than just one. Here it is observed that such an adaptation has a significant effect on the frequency dependency of the diffusion model. The effective cutoff frequency of the diffusion model is reduced as the number of layers is increased. For the MA90 case, for instance, the cutoff frequency is reduced from about 4000 Hz for the single-layer model, to 3150 Hz for the double-layer model and finally to 2000 Hz for the triple-layer model. Again, an upper limit is observed in the measured random incidence diffusion coefficient data for both adapted versions of the model, but with the threshold slightly greater than the single-layer case, at 0.69 for the double-layer model, and 0.73 for the triple-layer model. Future work will investigate the possibilities of controlling the

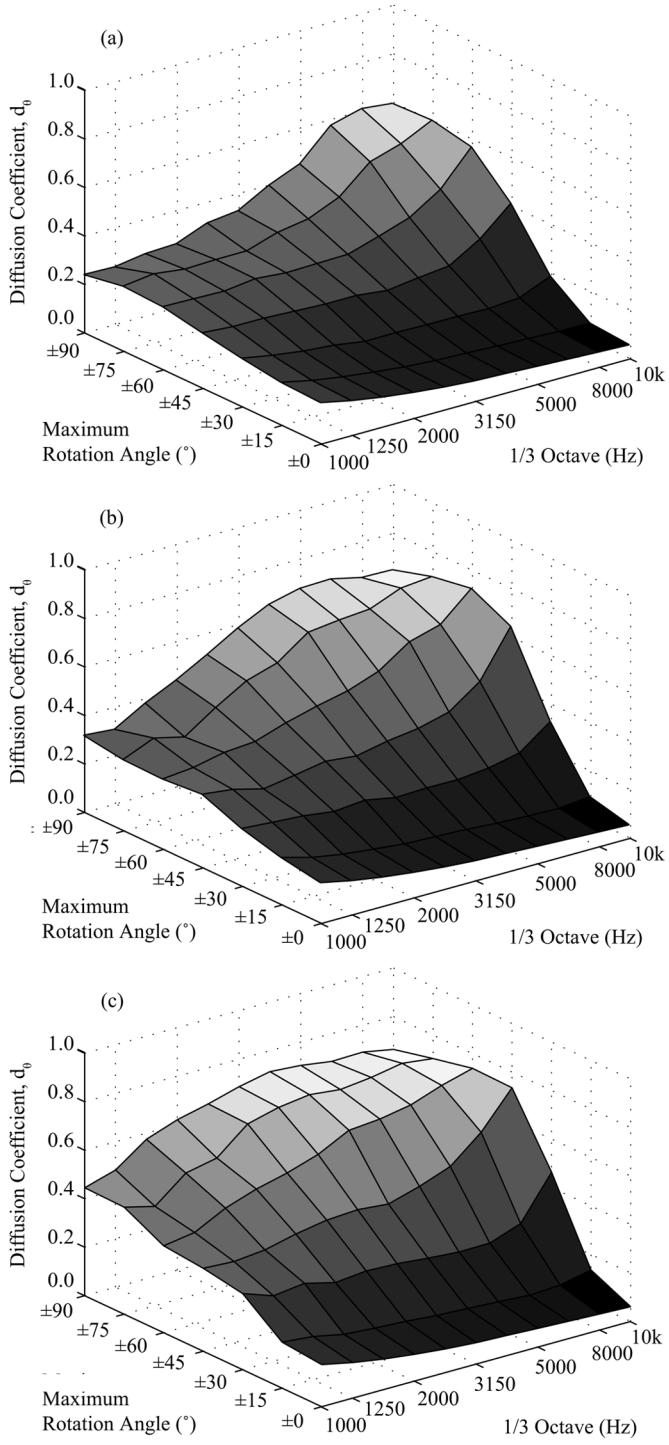

Fig. 15. Frequency-dependent random incidence diffusion coefficients for (a) single, (b) double, and (c) triple-layered adaptations of the diffusing layer model.

frequency dependency of the diffusing layer model using such an approach.

It is noted that the model is dependent on the sampling rate and the spatial distances between junctions in the DWM. Also, although it can be readily applied to other mesh topologies, its effect may vary depending on which topology it is implemented with. Therefore, further study is also required to investigate how the nature of the model changes under these different conditions.

TABLE II
TABLE SHOWING RT_{60} TIMES OF A DWM STRUCTURE AT DIFFERENT OCTAVE BANDS WITH EACH OF THE SEVEN DIFFUSION MODELS IMPLEMENTED AT ALL BOUNDARIES

Octave Band (Hz)	RT_{60} times MA 00	MA 15	MA 30	MA 45	MA 60	MA 75	MA 90
63	1.416	1.297	1.382	1.311	1.312	1.268	1.329
125	1.400	1.573	1.611	1.421	1.413	1.470	1.510
250	1.603	1.610	1.565	1.532	1.293	1.332	1.219
500	1.488	1.393	1.615	1.623	1.620	1.429	1.435
1000	2.014	1.885	1.869	1.806	1.773	1.681	1.643
2000	2.039	1.905	1.713	1.714	1.710	1.734	1.772
4000	2.243	2.219	1.724	1.786	1.775	1.768	1.820
8000	1.707	1.834	1.744	1.731	1.738	1.744	1.725

G. Effect on Absorption Filtering at Boundaries

The diffusion method described in this paper allows for the simultaneous application of frequency-dependent absorption filters at the boundary junctions of the digital waveguide mesh, because the boundary junctions themselves are not involved in the diffusion process. However, the nature of the model means that the energy of incident sound waves at a boundary is scattered both before and after the reflection. This potentially alters the way in which incident waves interact with the boundary filters when the diffusion method is implemented, compared to when it is not implemented. The greater the range of rotation angles used in the boundary scattering model, the greater the scattering of the sound wave energy and the greater this potential effect, with the possibility that some energy is scattered away from the incident direction completely and therefore does not interact with the boundary filter at all.

In order to test the effect of the diffusion method on boundary absorption filtering, a square DWM structure is constructed, with a side length of 4 m and sampling frequency f_{update} of 44.1 kHz. A series of seven simulations are then performed. In each simulation, the diffusing layer method, as described in Section V, is implemented at all boundaries of the structure. However, specific maximum rotation angles of $0°, \pm 15°, \pm 30°, \pm 45°, \pm 60°, \pm 75°$, and $\pm 90°$ are used for each subsequent simulation. Again, these modeled boundaries are referred to as MA00, MA15, MA30, MA45, MA60, MA75, and MA90, respectively. A simple boundary filter is also applied to all boundaries in the structure, designed to simulate an absorption coefficient of 0.05 at all octave bands with center frequencies from 62.5 Hz to 8 kHz.

In each simulation, three impulse responses are obtained by exciting the mesh with a low-pass filtered impulse near one corner and generating an output from a junction at random points elsewhere in the mesh. From these impulse responses, average RT_{60} values are calculated at octave bands according to [40]. The results, presented in Table II, show that the effect of increasing the maximum angle of rotation in the boundary diffusion model is inconsistent at different octave bands. Although some fluctuation is observed, in general the trend is for the RT_{60} values to decrease as the maximum rotation angle is increased. This fluctuation indicates that the effect of boundary absorption filters is potentially slightly attenuated as the maximum rotation angle increases.

There are other factors that must be considered that will affect the RT_{60} times given in this result. The main factor is that

the spread of energy away from the modal frequencies in the impulse response results in shorter decay times at these frequencies, as more boundaries are visited by this energy and the angle of incidence is more varied [6]. The slight increase in reverberation times at certain octave bands, caused by the increase in rotation angle of the diffuse boundary model can potentially be compensated for by increasing the absorption coefficient of the modeled boundary in these octave bands. A more extensive study is therefore required, to investigate the full effect of the diffusing layer model on the boundary absorption filtering. This is the subject of future work.

H. Computational Analysis

In order to test the added computational load that results from the diffusion boundary model presented in this paper, a simple rectangular DWM structure, exactly the same shape and size as that used for model A in Section VI-A is constructed. Again, the sample rate of the mesh is set at 44.1 kHz. An impulse is applied to the mesh and the processing time taken to perform a 2-s simulation is measured. The memory used by the DWM implementation is also measured. The test is performed first with the diffusing layer model applied at all boundaries (the maximum angle set at $\pm 45^{\circ}$) and then again with no diffusing layer model applied at all. The total number of scattering junctions in the structure (for both tests) is 20 201 junctions. The number of scattering junctions used for the diffusion model in the first test is 590, 2.92% of the total amount. The results show that when the diffusing layer model is implemented at all boundaries in the DWM, the increase in memory usage in this case is negligible (13 772 kb for both simulations). The execution time of the simulation without the diffusing layer implementation in this case is 1472.44 s. However, the total computation time with the diffusing layer implemented is slightly longer by 7.48 s (1479.92 s), an increase of only 0.508%.

VII. Conclusion

A method for modeling diffuse boundaries with controllable boundary scattering has been presented. The method has been analyzed in depth by implementing a range of boundary models in specific testing simulations. The results give useful information regarding the diffusivity of the models and show that the method is effective, as well as offering a high degree of user control. Diffusion coefficient results are valid for frequencies above 5% of the sampling frequency. Information regarding the diffusing layer model's scattering properties at lower frequencies can be acquired by increasing the length of the boundary sample under test, as well as increasing the relative distances between the boundary and the source and receivers. Results have shown that for a sampling frequency of 44.1 kHz, the model is most effective for frequencies over 5000 Hz. In the 8-kHz and 10-kHz 1/3 octave bands, an upper limit of 0.61 is observed in the measured random incidence diffusion coefficient data. The results indicate that the model is suitable for modeling small-scale, random irregularities with maximum sizes of between 3 and 8 cm. It is also shown that by adapting the model so that more than one single diffusing layer is applied, the model becomes effective for frequencies lower than 4000 Hz and the diffusion bandwidth of the model can be increased with higher measured random incidence diffusion coefficients. It cannot be compared with commercial diffusors, however, which are designed to give optimal diffusion over a specific bandwidth and whose diffusive characteristics are quite different to randomly irregular boundaries as a result. Note also that professional diffusors are typically designed to work at frequencies between about 500 Hz and 5 kHz. Above 5 kHz, natural surface roughness will often be sufficient for boundary diffusion.

Future work will concentrate on the simulation of frequency dependent diffuse boundaries and the extension of the diffusion model to 3-D DWMs. Further acquisition of diffusion coefficient data is planned, so that frequency-dependent diffuse boundaries can be accurately designed and implemented in DWM simulations given their diffusion coefficients. The effect of applying the model to meshes of different sampling rates and different mesh topologies on its diffusive behavior in general will also be investigated. Finally, a more detailed study is planned of the effect of the diffusing layer model on the implementation of boundary absorption in the DWM.

References

[1] A. Krokstad, S. Strøm, and S. Sørsdal, "Calculating the acoustical room response by the use of a ray tracing technique," *J. Sound Vibration*, vol. 8, no. 1, pp. 118–125, 1968.

[2] J. B. Allen and D. A. Berkley, "Image method for efficiently simulating small-room acoustics," *J. Acoust. Soc. Amer.*, vol. 65, pp. 943–950, 1979.

[3] L. Savioja, T. J. Rinne, and T. Takala, "Simulation of room acoustics with a 3-D finite difference mesh," in *Proc. Int. Comput. Music Conf.*, 1994, pp. 463–466.

[4] D. T. Murphy and M. J. Beeson, "Modelling spatial sound occlusion and diffraction effects using the digital waveguide mesh," in *Proc. AES 24th Int. Conf.—Multichannel Audio*, Alberta, BC, Canada, Jun. 2003, pp. 207–216.

[5] F. A. Everest, *Master Handbook of Acoustics*. New York: McGraw-Hill, 2001.

[6] J. A. S. Angus, A. C. Marvina, J. Clegg, J. Dawson, and A. Knobloch, "The effect of acoustic diffusers on room mode decay," in *Proc. 99th Convention Audio Eng. Soc.*, New York, Oct. 1995, preprint 4116.

[7] D. E. Hall, *Musical Acoustic, An Introduction*. Belmont, CA: Wadsworth, 1980.

[8] *Acoustics—sound-scattering properties of surfaces—Part 1: Measurement of the random-incidence scattering coefficient in a reverberation room*, Std. ISO 17 497-1:2004, Int. Org. Standardization, 2004.

[9] *AES information document for room acoustics and sound reinforcement systems—Characterization and measurement of surface scattering uniformity*, Std. AES-4id-2001, Audio Eng. Soc., 2001.

[10] T. J. Cox, B.-I. L. Dalenback, P. D. Antonio, J. J. Embrechts, J. Y. Jeon, E. Mommertz, and M. Vorländer, "A tutorial on scattering and diffusion coefficients for room acoustic surfaces," *Acta Acustica United with Acustica*, vol. 92, no. 1, pp. 1–15, 2006.

[11] H. Nironen, "Diffuse reflections in room acoustic modelling," M.S. thesis, Helsinki Univ. of Technol., Espoo, Finland, 2004.

[12] H. Kuttruff, "Simulierte nachhallkurven in rechteckraumen mit diffusem schallfeld," *Acustica*, vol. 25, pp. 333–342, 1971.

[13] K. Lee and J. O. Smith, "Implementation of a highly diffusing 2-D digital waveguide mesh with a quadratic residue diffuser," in *Proc. Int. Comput. Music Conf. (ICMC)*, Miami, FL, Nov. 2004, pp. 309–315.

[14] J. Laird, P. Masri, and N. Canagarajah, "Modelling diffusion at the boundary of a digital waveguide mesh," in *Proc. Int. Comput. Music Conf.*, Hong Kong, Oct. 1999, pp. 492–495.

[15] S. Shelley and D. T. Murphy, "Diffusion modelling at the boundary of a digital waveguide mesh," in *Proc. 13th Eur. Signal Process. Conf.*, Antalya, Turkey, Sep. 2005 [Online]. Available: http://www.ee.bilkent.edu.tr/~signal/defevent/papers/cr1397.pdf , paper CR1397

[16] S. Shelley and D. T. Murphy, "Measuring diffusion in a 2-D digital waveguide mesh," in *Proc. 8th Int. Conf. Digital Audio Effects (DAFx'05)*, Madrid, Spain, Sep. 2005, pp. 249–253.

[17] J.-P. Berenger, "A perfectly matched layer for the absorption of electromagnetic waves," *J. Comput. Phys.*, vol. 114, no. 2, pp. 185–200, Oct. 1994.

[18] T. J. Cox and P. D'Antonio, *Acoustic Absorbers and Diffusers: Theory, Design and Application*. Oxon, U.K.: Spon Press, 2004.

[19] J. H. Rindel, "Attenuation of sound reflections due to diffraction," in *Proc. Nordic Acoust. Meeting*, Aalborg, Denmark, 1986, pp. 257–260.
[20] J. O. Smith, "Physical modelling using digital waveguides," *Comput. Music J.*, vol. 16, pp. 74–87, Winter, 1992.
[21] J. O. Smith, , M. Kahrs and K. Brandenburg, Eds., *Principles of Digital Waveguide Models of Musical Instruments*. Boston, MA: Kluwer, 1998.
[22] P. B. Johns and R. L. Beurle, "Numerical solution of two-dimensional scattering problems using a transmission-line matrix," *Proc. IEEE*, vol. 118, no. 12, pp. 1203–1209, Dec. 1971.
[23] S. Bilbao, *Wave and Scattering Methods for Numerical Simulation*. Chichester, U.K.: Wiley, 2004.
[24] J. Escolano and F. Jacobsen, "A note on the physical interpretation of frequency dependent boundary conditions in a digital waveguide mesh," *Acta Acustica United With Acustica*, vol. 93, no. 3, pp. 398–402, May/Jun. 2007.
[25] D. T. Murphy, "Digital Waveguide Mesh Topologies in Room Acoustics Modelling" Ph.D. dissertation, Univ. of York, York, U.K., 2000 [Online]. Available: http://www-users.york.ac.uk/dtm3/Download/ThesisTotal.pdf
[26] M. Karjalainen and C. Erkut, "Digital waveguides versus finite difference structures: Equivalence and mixed modeling," *EURASIP J. Appl. Signal Process.*, vol. 7, pp. 978–989, Jun. 2004.
[27] D. T. Murphy and M. J. Beeson, "The KW-boundary hybrid digital waveguide mesh for room acoustics applications," *IEEE Trans. Audio, Speech, Lang. Process.*, vol. 15, no. 2, pp. 552–564, Feb. 2007.
[28] D. T. Murphy and D. M. Howard, "2-D digital waveguide mesh topologies in room acoustics modelling," in *Proc. Cost G-6 Conf. Digital Audio Effects*, Verona, Italy, Dec. 2000, pp. 211–216.
[29] S. A. V. Duyne and J. O. Smith, "The 3-D tetrahedral waveguide mesh with musical applications," in *Proc. Int. Comput. Music Conf.*, Hong Kong, 1996, pp. 9–16.
[30] L. Savioja and V. Välimäki, "Reducing the dispersion error in the digital waveguide mesh using interpolation and frequency warping techniques," *IEEE Trans. Speech Audio Process.*, vol. 8, no. 2, pp. 184–193, Mar. 2000.
[31] L. Savioja and V. Välimäki, "Interpolated rectangular 3-D digital waveguide mesh algorithms with frequency warping," *IEEE Trans. Speech Audio Process.*, vol. 11, no. 6, pp. 783–789, Nov. 2003.
[32] S. A. V. Duyne and J. O. Smith, "Physical modeling with the 2-D digital waveguide mesh," in *Proc. Int. Comput. Music Conf.*, Tokyo, Japan, 1993, pp. 40–47.
[33] D. Rocchesso and J. Smith, "Circulant feedback delay networks for sound synthesis and processing," in *Proc. Int. Comput. Music Conf.*, 1994, pp. 378–381.
[34] J. Stautner and M. Puckette, "Designing multichannel reverberators," *Comput. Music J.*, vol. 6, no. 1, pp. 52–65, Spring, 1982.
[35] J. M. Jot and A. Chaigne, "Digital delay networks for designing artificial reverberators," in *Proc. 90th Conv. Audio Eng. Soc.*, Paris, France, Feb. 1991, preprint 3030.
[36] P. J. Davis, *Circulant Matrices*. New York: Wiley, 1979.
[37] D. Rocchesso and J. O. Smith, "Circulant and elliptic feedback delay networks for artificial reverberation," *IEEE Trans. Speech Audio Process.*, vol. 5, no. 1, pp. 51–63, Jan. 1997.
[38] R. M. Gray, *Toeplitz and Circulant Matrices: A Review*. Hanover, MA: Now, 2006.
[39] S. Shelley, "Audio demonstration of the diffusion layer model," Nov. 2005 [Online]. Available: http://www-users.york.ac.uk/~dtm3/diffusion.html
[40] *Acoustics—Measurement of Reveberation Time of Rooms with Reference to Other Acoustical Parameters*, Std. ISO 3382:2000, Int. Org. for Standardization, 2000.

Simon Shelley received the M.Eng. degree in electronic engineering with music technology systems from the University of York, York, U.K., in 2003. He is currently working towards the Ph.D. degree on the accurate modeling of acoustic boundaries in the digital waveguide mesh, which is to be completed in 2008.

His research interests include acoustic modeling, sound spatialization, and human–computer interaction for musical applications.

Damian Murphy received the B.Sc. (hons.) degree in mathematics, the M.Sc. degree in music technology, and the D.Phil. degree in music technology from the University of York, York, U.K., in 1993, 1995, and 2000, respectively.

In 1999, he was Lecturer in Music Technology in the School of Engineering, Leeds Metropolitan University, Leeds, U.K., and in 2000 was appointed as Lecturer in the Department of Electronics, University of York. He has worked as Audio Consultant and since 2002 has been a Visiting Lecturer in the Department of Speech, Music, and Hearing, KTH, Stockholm, Sweden. His research is in the areas of physical modeling and spatial sound, with particular interests in applications of the multidimensional digital waveguide mesh. He is an active composer in the fields of electroacoustic and electronic music, where sound spatialization forms a critical aspect of his musical works. In 2004, he was appointed as one of the U.K.'s first AHRC/ACE Arts and Science Research Fellows, investigating the compositional and aesthetic aspects of sound spatialization and acoustic modeling techniques.

Dr. Murphy is a member of the Audio Engineering Society.